Received: 5 December 2025 | Revised: 3 February 2026 | Accepted: 18 February 2026

DOI: 10.1002/mp.70391

RESEARCH ARTICLE

MEDICAL PHYSICS

Real-time energy measurement of clinical carbon ion beams using a cross-correlation time-of-flight method with parallel-plate chambers

Na Hye Kwon[1] | **Sung Woon Choi**[1] | **Soorim Han**[1] | **Yongdo Yun**[1] | **Min Cheol Han**[1] | **Chae-Seon Hong**[1] | **Ho Jin Kim**[1] | **Ho Lee**[1] | **Changhwan Kim**[1] | **Do Won Kim**[1] | **Woong Sub Koom**[1] | **Jin Sung Kim**[1,2] | **Nuno Carolino**[3] | **Luis Lopes**[3] | **Dong Wook Kim**[1,4] | **Paulo J. R. Fonte**[1,3,5]

[1]Department of Radiation Oncology, Yonsei Cancer Center, Heavy Ion Therapy Research Institute, Yonsei University College of Medicine, Seoul, Republic of Korea

[2]Oncosoft Inc., Seoul, South Korea

[3]LIP – Laboratory of Instrumentation and Experimental Particle Physics, Coimbra, Portugal

[4]ARA Inc., Seoul, South Korea

[5]Coimbra Institute of Engineering, Polytechnic University of Coimbra, Coimbra, Portugal

Correspondence
Dong Wook Kim, Department of Radiation Oncology, Yonsei Cancer Center, Yonsei University College of Medicine, 50–1 Yonsei-ro, Seodaemun-gu, Seoul 03722, Republic of Korea.
Email: joocheck@gmail.com

Paulo J. R. Fonte, LIP–Laboratory of Instrumentation and Experimental Particle Physics, Rua Larga, Coimbra 3004–516, Portugal.
Email: fonte@lip.pt

Funding information
Korea Institute for Advancement of Technology, Grant/Award Number: P0026103; National Research Foundation of Korea, Grant/Award Number: RS-2024-00410034; Korea Foundation Of Nuclear Safety (KOFONS), Grant/Award Number: 2205013

Abstract

Background: In carbon-ion radiotherapy (CIRT), the beam energy determines both the particle range and the overall dosimetric quality. Range-verification QA devices such as Zebra and Giraffe, which are based on multilayer ionization chambers (MLICs), can verify the range but only under dedicated QA conditions, leaving any energy deviations introduced by nozzle components undetected in real time. In particular, nozzle structures such as ridge filters can broaden or modulate the energy spectrum, causing the effective energy delivered to the patient to differ from the nominal accelerator setting. These limitations highlight the need for a real-time method capable of verifying the beam energy under actual clinical operating conditions.

Purpose: We proposed a TOF-based beam-energy measurement concept that leverages a cross-correlation analysis of full detector waveforms. Compact and radiation-hard parallel-plate chambers (PPCs) were developed and evaluated, in contrast to prior TOF systems based on semiconductor detectors.

Methods: PPCs (2.5 cm diameter active area, 0.4 mm gas gap) were operated in CO_2. Two detectors were mounted coaxially with detector separations of 22.5 and 46.3 cm. Experiments were performed at Yonsei Heavy-ion Therapy Center (HITC) using four nominal energies (102.6, 140.4, 250.3, 430 MeV/nucleon) and three intensities, covering the clinically interesting ranges. Signals were digitized with a 1 GHz bandwidth oscilloscope. For each spill, paired waveforms were cross-correlated, and peak times were refined by parabolic interpolation to determine TOF. Precision and accuracy were evaluated across energies, intensities, and detector separations.

Results: The PPCs operated stably for all beam conditions. Under pencil-beam delivery and normalized to 1 s acquisitions, the timing precision of the mean TOF (standard error) remained within 1 ps for both detector separations, scaling with $1/\sqrt{N}$ (N: number of TOF samples per acquisition) and not representing the single-particle TOF resolution. Residuals between measured and theoretical TOF remained within 80 ps across energies and distances. After relativistic conversion from TOF to kinetic energy and then to water-equivalent range, all deviations were within a 1 mm range shift, meeting the recommended clinical criteria for range verification.

Conclusions: We demonstrated that compact CO_2-filled PPCs, operated as a TOF pair, can measure carbon-ion beam energy across the clinically relevant range of energies (≈100–430 MeV/u) and intensities used in routine treatment delivery. We achieved sub-picosecond timing precision on the TOF mean (standard error) per 1 s acquisition and submillimeter water-equivalent range accuracy using a robust cross-correlation analysis method. These results open the way to the integration of PPC-based TOF monitoring to tighten beam-delivery tolerances and improve the reliability and safety of carbon-ion radiotherapy.

KEYWORDS
carbon-ion radiotherapy, cross-correlation, energy monitoring system, parallel-plate chamber, time-of-flight

1 | INTRODUCTION

Carbon-ion radiotherapy (CIRT) is an advanced technique of radiation therapy that leverages the physical advantage of the Bragg peak and the high relative biological effectiveness (RBE) of carbon-ions.[1,2] Its clinical adoption has been steadily expanding worldwide in response to the growing demand for more precise and effective cancer treatment. The first CIRT facility, HIMAC, was established in Japan, and as of today, more than 20 centers are operational or under construction worldwide.[3,4] CIRT offers substantial benefits over conventional photon therapy by delivering highly conformal dose distributions that spare surrounding healthy tissues and organs. Moreover, clinical studies have reported favorable outcomes with improved tumor control and survival, particularly in radioresistant cancers such as lung, head and neck, and mucosal melanoma.[5–8]

Synchrotron-based CIRT systems constitute complex infrastructures integrating multiple precision control technologies for real-time beam quality management. Key physical parameters—such as beam position, dose, intensity, and energy—are regulated through dedicated hardware and control systems, and monitored by detectors strategically installed between the injector, accelerator, and high-energy beam transport (HEBT) sections.[9] These control mechanisms are based on technologies first developed at HIMAC and later adopted in Toshiba synchrotrons.[10–13] In particular, Toshiba systems employ multi-energy operation using RF modulation and beam-chopper control, enabling precise regulation of energy and intensity, energy selection across 600 discrete steps, and beam intensity.[11–13]

Although modern CIRT systems provide highly precise control of beam delivery parameters, efforts have increasingly focused on establishing independent methods for direct verification of beam energy and range. Several approaches have been proposed, including real-time monitoring techniques implemented downstream of the nozzle to complement conventional QA procedures.[14–16] In addition to these clinical developments, TOF-based detector concepts have been extensively used in high-rate experimental environments such as large-scale particle- and neutron-physics facilities, where precise timing and energy determination over long flight paths are required.[17,18] In this context, our work aims to explore a time-of-flight (TOF)–based strategy for carbon-ion beam-energy measurement under clinical beam conditions. Among TOF-based attempts more directly related to beam QA in a clinical scenario, solid-state detector systems have shown promising results, particularly in proton therapy, where ultrafast silicon detectors (UFSDs) have been employed for absolute beam-energy determination.[19,20] However, their limited radiation hardness and the high cost of large-area implementations are likely to limit their practical applicability in carbon-ion therapy.

As an advantageous alternative, previous work has shown that a parallel-plate chamber (PPC) can achieve picosecond-level timing precision under clinical beam conditions.[21] In this work, we implemented a dual-PPC TOF setup on the same beam to directly measure the absolute beam energy and evaluate whether its precision meets the clinical goal of ± 1 mm in water-equivalent range.

2 | MATERIALS AND METHODS

2.1 | Experimental setup

The TOF measurement system used in this study consisted of two PPC detectors positioned sequentially along the beam axis. The detectors were mounted with an adjustable separation and operated with independently applied bias voltages to accommodate different measurement configurations. As shown in Figure 1a, the two PPCs were installed at fixed separations depending on the experimental configuration.

Each PPC had a circular active area with a diameter of 2.5 cm and a uniform gas gap of 0.4 mm. Both detectors were mounted at the center of a gastight box, highlighted by the cyan dotted region in Figure 1a. Owing

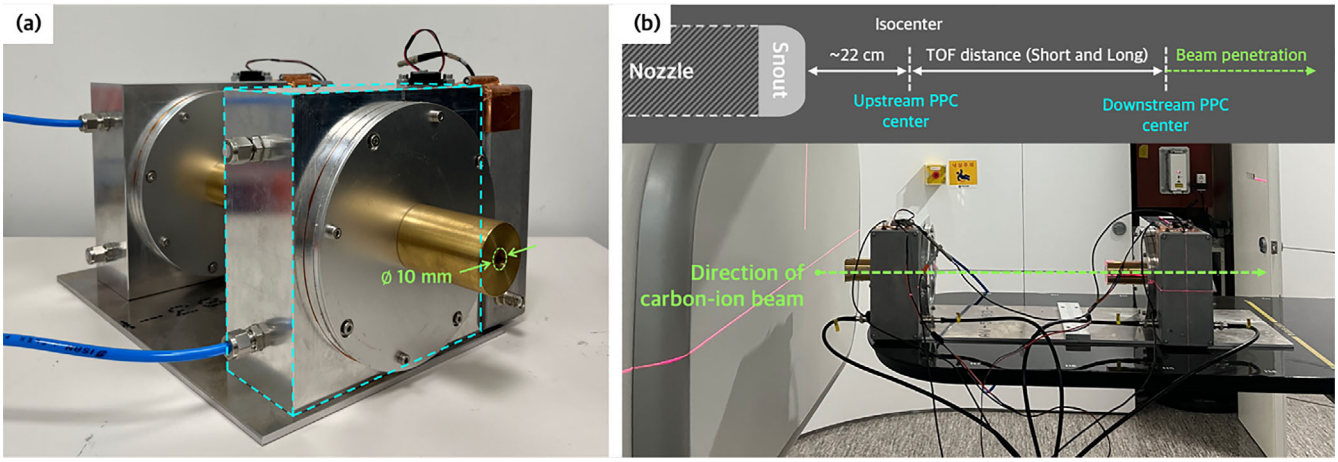

FIGURE 1 (a) Dual PPC assembly for TOF measurements, each with a Ø10 mm brass collimator positioned upstream of the active area (cyan dotted box: gastight housing). (b) Schematic and in-room setup at Yonsei HITC, showing the PPC arrangement for short (22.5 cm) and long (46.3 cm) TOF configurations.

to the relatively small active area, we constrained the beam to pass only through the center of the active area by using a brass collimator of 10 mm internal diameter and 60 mm length placed just upstream from each chamber, as illustrated in Figure 1a.

Prior to the experiment the chambers were filled with pure CO_2, and during operation the system was maintained sealed. Each chamber was biased with a voltage of 1570 V, corresponding to an electric field of 39.25 kV/cm across the 0.4 mm gap.

To protect sensitive equipment such as the digital oscilloscope and the high-voltage power supplies from secondary particles exposure, these devices were placed outside the treatment room in a maze-structured service corridor. Therefore, the amplified signals were transmitted to the oscilloscope via 20 m-long LEMO cables. Signal acquisition was performed using a Teledyne LeCroy HDO6104B digital oscilloscope (1 GHz bandwidth, 12-bit resolution) at a 1.25 GSPS rate. The acquisition was triggered by simple thresholding of the signals present on either PPC and a 20 ms long sweep was acquired for each trigger. All acquired waveforms were stored in binary format for offline analysis.

2.2 | Carbon beam experiment condition

The experiments were conducted at the Yonsei Heavy-ion Therapy Center (HITC, Seoul, Republic of Korea) using a synchrotron-based CIRT system (CI-1 000, Toshiba, Japan).[9] The in-beam experimental setup is shown in Figure 1b. The PPCs were installed along the beam axis, with the upstream detector aligned with the isocenter. The selected nominal energies (102.56, 140.44, 250.25, 430.00 MeV/nucleon, MeV/u) correspond to water-equivalent penetration depths ranging from approximately 1 cm to over 30 cm, effectively covering the range required for most clinical treatment cases. The beam parameters—including nominal energy, expected energy in the space between the PPCs and average particle rate—are summarized in Table 1. The average particle rates listed in Table 1 correspond to the expected rates on the upstream PPC after the 10 mm brass collimator for each energy–intensity combination.

The detector separations were set to (nominally) 22.5 cm ("Short") or 46.3 cm ("Long"), respectively. The irradiation plan was configured such that the beam-on time was set to 15 s for each energy–intensity condition, ensuring consistent data acquisition windows across all settings.

2.3 | Data processing and cross-correlation analysis

Each 20 ms long sweep was digitally filtered by a rectangular digital bandpass filter accepting from 10 to 200 MHz, empirically chosen as the optimal range. Each sweep was subdivided into 10 000 segments, each 2 µs in duration. Each segment was analyzed independently and yielded one TOF measurement. This subdivision level was empirically determined to deliver the best overall TOF precision.

For each segment the signal was 10-fold interpolated to improve the time granularity and the TOF was computed by applying a cross-correlation algorithm between the two interpolated signals.[21–23] One signal was incrementally shifted in time relative to the other and their correlation was evaluated for each offset. The temporal offset corresponding to the peak of the cross-correlation function was defined as the TOF measurement. To identify the peak a second-order polynomial was fitted to the 7 samples surrounding the offset value with the highest correlation and the peak was defined as the maximum of this polynomial, allowing for analog-level resolution on the peak position. An illustration of the

TABLE 1 Beam settings used for TOF measurements at Yonsei HITC. The nominal energy (K_0) is the machine setting from the "Energy ID" (EID); the measured R_{80} range with PPC is the corresponding beam range value measured by the Giraffe device with interposed PPC; the kinetic energy after PPC (K) is the expected energy after passing through the upstream PPC, estimated by simulation as part of the dosimetry procedure. Three intensity levels (low/medium/high) were delivered, and the average particle rate as estimated for each level.

Nominal energy (K_0) (MeV/u)	Measured R_{80} range with PPC (R) (mm)	Kinetic energy (K) after PPC (MeV/u)	Intensity	Average particle rate (s^{-1})
102.56	13.661	70.90	Low	2.20E + 07
			Medium	1.24E + 08
			High	2.34E + 08
140.44	33.325	116.23	Low	2.76E + 07
			Medium	1.56E + 08
			High	2.94E + 08
250.25	113.32	234.56	Low	4.13E + 07
			Medium	2.34E + 08
			High	4.40E + 08
430.00	295.16	418.63	Low	5.65E + 07
			Medium	3.20E + 08
			High	6.03E + 08

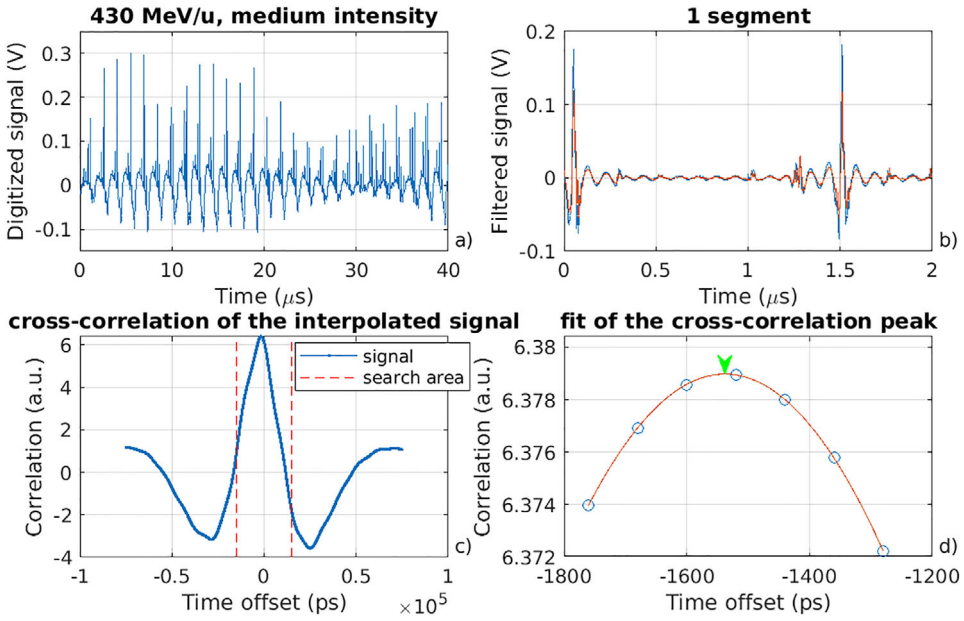

FIGURE 2 Illustration of the analysis procedure: (a) Raw signal, as digitized (the full sweep is 20 ms long); (b) One 2 μs long segment after band-pass digital filtering; (c) Cross-correlation function between the two signals in the segment; (d) Parabolic fit around the correlation peak, the vertex (green arrow) indicates the measured time offset.

successive steps of this procedure can be found in Figure 2.

2.4 | Signal-strength correction and TOF distribution analysis

To quantify the signal strength in each segment, the root mean square (RMS) values of both PPC signals were computed and summed. A weak but consistent dependence of TOF on the signal strength was observed across all beam energies and detector separations, suggesting a systematic bias potentially arising from detector or readout characteristics. To mitigate this effect, a linear regression was performed on the TOF versus. RMS distribution for each energy and distance, therefore amalgamating all intensities together for each energy-separation combination. TOF values were then extrapolated to the zero-amplitude limit, effectively correcting for strength-dependent shifts. This procedure is

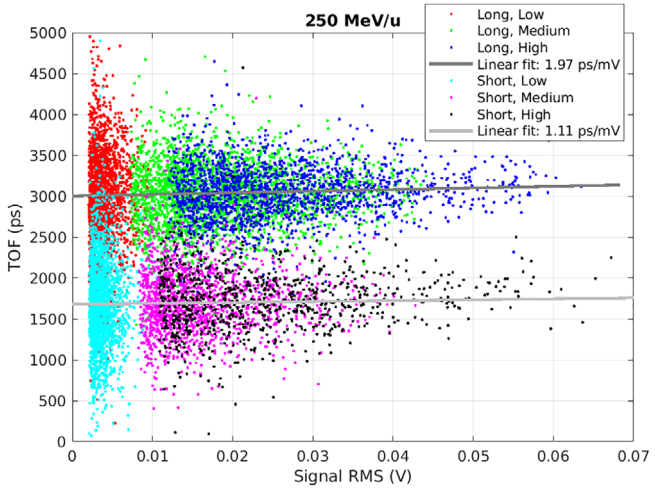

FIGURE 3 Correlation between the summed RMS signal strengths from both PPCs and measured TOF at 250 MeV/u. Data are grouped by detector separation (long, short) and beam intensity (low, medium, high). Linear fits for each separation yield slopes of 1.97 ps/mV (long) and 1.11 ps/mV (short), illustrating an amplitude-dependent timing shift attributable to detector characteristics.

illustrated in Figure 3. Note that this is a calibration procedure that can be performed prior to any eventual clinical use. The very wide range of signal strengths visible in Figure 3 results from the intense modulation of the beam that occurs during normal accelerator operation.[21]

The slope of the dependency is reversed when the order of the chambers is reversed, indicating that this effect is tied to the chambers themselves and not to their position in the beam line. It was determined that when the applied voltage is varied in one of the chambers the measured TOF shifts by 1.3 ps/V, so it is conceivable that the dependency could be removed by a differential adjustment of the applied voltages.

Following this correction, TOF distributions were constructed for each combination of beam energy and detector separation using the signal-strength–corrected TOF values obtained on a segment-by-segment basis. To robustly estimate a representative TOF value for each energy–separation pair, a truncated logistic function was fitted to the cumulative distribution of these corrected TOF measurements. The representative TOF value was defined as the midpoint (50% level) of the fitted cumulative distribution, corresponding to the inflection point of the logistic function.[21] This approach provides a stable estimate of the central TOF value that is less sensitive to outliers and non-Gaussian tails than a simple mean.

2.5 | Evaluation of the TOF measurements

To evaluate the performance of the PPC-TOF system, we assessed both timing precision (intra-condition consistency) and accuracy (agreement with an independent estimation). Timing precision was quantified as one quarter of the width of the 95% confidence bounds for the mode as determined by the fitting procedure mentioned above. As the precision of the mode depends inversely on the square root of the number of measurements, the quoted precisions were converted to an equivalent measurement time of 1 s. In Yonsei HITC clinical practice each "energy layer" corresponds to several hundreds of milliseconds, so a 1 s measurement time corresponds to the same order of magnitude in precision.

At Yonsei HITC the fundamental spill period is around 1 μs so in a 1 s measurement time about 1 million spills will be measured.[21] Of course, in other facilities the beam time structure may vary, with an impact on precision that can't be foreseen by us.

For accuracy determination the measurement was compared with an independent estimation of three parameters: TOF, kinetic energy and range in water. Of these, range in water (r) is the most clinically relevant and it is directly measured for a wide range of nominal energies (k_0) as part of the regular quality assurance of the facility, defining experimentally the function $r(k_0)$. At this facility r is defined as the distance at which the energy deposition density drops to 80% of its peak value (Bragg peak). Note that the nominal energies are very sharply defined by the accelerator revolution frequency and are a reliable reference for the beam energy generated by the accelerator, but, as discussed above, this doesn't correspond exactly to the energy at the delivery point.

From the measured energy deposition curves in water the average kinetic energy of the beam, k, is estimated by fitting these curves by simulation for each $\{k_0, r\}$ pair. The function $k(r)$ is available as part of the normal dosimetry procedure and from it we defined numerically the inverse function $r(k)$. Both functions were implemented as an interpolation between the data points presented in Table 1 by a shape-preserving cubic polynomial, continuous to the first derivative.

It should be noted that it is unclear which procedure is more accurate: kinetic energy measurement from TOF, a rather direct measurement, or kinetic energy estimation from the water range curves, which is very indirect because it involves simulation of the beam interaction with water and requires assumptions about the beam energy spectrum.

There is an experimental complication arising from the non-negligible thickness of the PPCs, which causes the beam energy in the space between the PPC pair to be smaller than what it should be for the nominal energies at which the $r(k_0)$ function was measured. To account for this effect, we measured the water ranges (R) at the nominal energies used (K_0) when the PPC is placed upstream of the IBA Giraffe (IBA Dosimetry, Schwarzenbruck, Germany).[24] The PPC

water-equivalent thickness was found to be close to 6.2 mm for all energies of interest. The "Expected kinetic energy" for each K_0 is then $K = k(R)$ and the values are listed in Table 1.

To convert from TOF (t) to kinetic energy, $k(t, d)$, and vice-versa, $t(k, d)$, we use the relativistic expressions,[19] where E_0 is the rest energy per nucleon (930.983 MeV/u):

$$k(t,d) = E_0\left(\frac{1}{\sqrt{1-\left(\frac{d}{c\cdot t}\right)^2}} - 1\right),$$
$$t(k,d) = \frac{(k+E_0)\cdot d}{c\sqrt{(k+E_0)^2 - {E_0}^2}} \quad (1)$$

being d the separation between detectors.

Together, these functions allow to convert the measurements from TOF to water range via kinetic energy and vice-versa. There are 3 ill-known calibration constants that must be experimentally determined: the effective detector separations in the two experimental configurations (D_{long} and D_{short}, respectively), and a global TOF time offset (C) that accounts for unknown contributions from cable lengths, electronics delays, and similar effects. These three constants were determined by a least-squares minimization of the function

$$\chi^2 = \sum_i \left[r\left(k\left(TOF_{i,short} + C, D_{short}\right)\right) - R_i\right]^2 + \sum_i \left[r\left(k\left(TOF_{i,long} + C, D_{long}\right)\right) - R_i\right]^2 \quad (2)$$

where the index i indicates the nominal energies. The fit was restricted to the points at nominal energies 140.44 MeV/u and 430.00 MeV/u, which correspond to the limits of the clinically useful range. The other two energies can be seen as validation points.

Note that this is a calibration procedure that can be performed prior to any eventual clinical use.

3 | RESULTS

Measured TOF precision and accuracy across the nominal energy range (100–430 MeV/u) were compared with theoretical predictions from relativistic kinematics (Figures 3 and 4).

In Figure 4 (top panel), measured flight times ($T = TOF + C$) for each expected kinetic energy K in both Long and Short detector separations are overlaid with theoretical values calculated from Equation (1). The x-axis represents the expected kinetic energy K (MeV/u), and the y-axis represents the measured TOF + cte (ps), where cte is the constant time offset determined by the least-squares minimization mentioned above. The middle panel presents the residuals ($\Delta T = T - T_{exp}$, $T_{exp} = t(K, D)$) between measured and theoretical TOF values, where D denotes the adjusted detector separation corresponding to each experimental configuration (Short or Long). Except for the lowest energy in the Long configuration, residuals remained within ± 20 ps.

The bottom panel of Figure 4 shows the TOF precision (Σ) and the corresponding water-equivalent range shift, calculated as $r(k(T, D)) - r(k(T + \Sigma, D))$. The Long configuration achieved precisions of 0.4–0.7 ps, corresponding to range uncertainties of 0.01–0.5 mm. The Short configuration improved precision to 0.4–0.5 ps, consistently maintaining submillimeter range uncertainties (0.01–0.8 mm) across the full energy range as summarized in Table 2.

Measured TOF values were then converted to absolute kinetic energies using the relativistic relation $k(t, d)$ and then to water-equivalent ranges (Figure 5). The top panel shows the kinetic energy error $\Delta K = k(T, D) - K$ as a function of K. The error bars correspond to the precision of the measurement, $k(T, D) - k(T + \Sigma, D)$ and represent the K uncertainty listed in Table 2. For both configurations, deviations were below ± 1 MeV/u, except at 102.56 MeV/u-Long configuration where an overestimation of 2.48 MeV/u was observed.

The bottom panel of Figure 5 presents the water range error, $\Delta R = r(k(T, D)) - R$, with error bars corresponding to the range shift already shown in Figure 4 (bottom panel). The error-bar values correspond to the Range uncertainty reported in Table 2. Across all beam energies and detector separations, the water-equivalent range error remained within ± 1.0 mm, thus satisfying clinical criteria for beam range verification.

4 | DISCUSSION

In this study, we experimentally validated a TOF system based on PPC detectors for measuring the average energy of carbon-ion beams. Previous studies have demonstrated that PPC detectors can achieve excellent timing performance, and the present results confirm that this capability supports TOF-based energy determination under clinical beam conditions.[21] To our knowledge, this is the first study to validate a cross-correlation signal analysis for carbon-ion energy measurement.

The proposed system features a simple and compact design, achieving sufficient timing resolution without the need for high-cost fast electronics. These advantages suggest its potential utility as a direct energy verification tool in routine quality assurance (QA), supplementing conventional range-based detectors. With further hardware optimization, the system may be extended to support real-time energy monitoring applications.

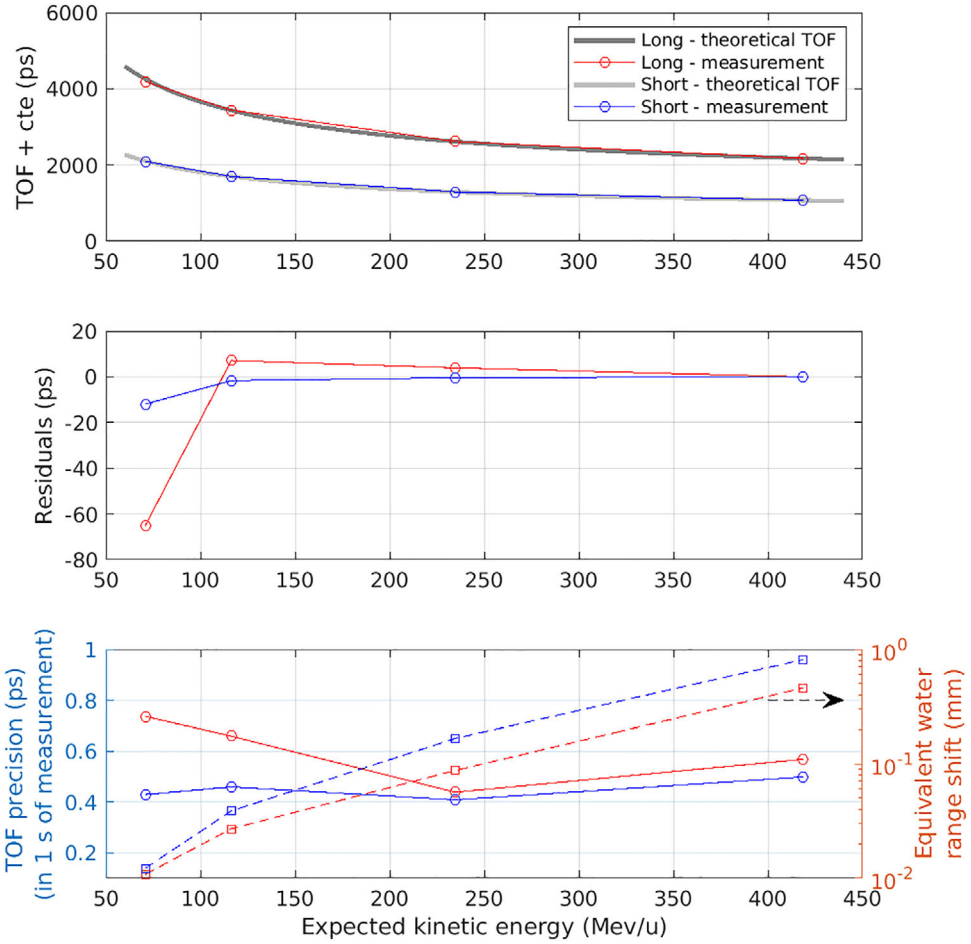

FIGURE 4 (Top) Measured TOF for long and short detector separations overlaid with theoretical values as a function of the expected kinetic energy. The *y*-axis shows the measured TOF plus a constant time offset *cte* denotes the global time offset determined in the calibration. (Middle) Residuals between measurement and theory. (Bottom) TOF precision and corresponding water-equivalent range shift.

TABLE 2 List of accuracy and precision results of measured TOF values for the two flight distances (23 and 47 cm) in the Yonsei HITC beam test. Fitted detector separations (long and short) and the global TOF offset were estimated by a global least-squares fit minimizing range error across all eight energy–Distance combinations. The table reports TOF accuracy and PPC-derived kinetic-energy error and water-equivalent range error with corresponding precision.

Distance configuration		Expected value		TOF			Kinetic energy		Range	
Nominal (cm)	Fitted (cm)	Kinetic energy, K (MeV/u)	TOF, T_{exp} (ps)	T, (ps)	Residual TOF, ΔT (ps)	TOF precision Σ (ps)	K Error, ΔK (MeV/u)	K uncertainty (MeV/u)	Range error, ΔR (mm)	Range uncertainty (mm)
22.5	23.29	70.9	2091.8	2103.7	−11.9	0.607	0.907	0.0466	0.334	0.0172
		116.23	1695.9	1697.6	−1.67	0.649	0.274	0.107	0.140	0.0547
		234.56	1291.5	1292.0	−0.465	0.577	0.238	0.296	0.189	0.235
		418.63	1073.7	1073.7	0.0704	0.704	−0.00978	0.977	−0.0115	1.15
46.5	47.11	70.9	4188.6	4253.6	−65.1	1.04	2.49	0.0409	0.921	0.0153
		116.23	3439.5	3432.5	7.08	0.932	−0.571	0.0748	−0.291	0.0382
		234.56	2616.3	2612.3	3.89	0.620	−0.981	0.156	−0.776	0.123
		418.63	2170.9	2170.9	−0.0290	0.803	0.0199	0.550	0.0234	0.649

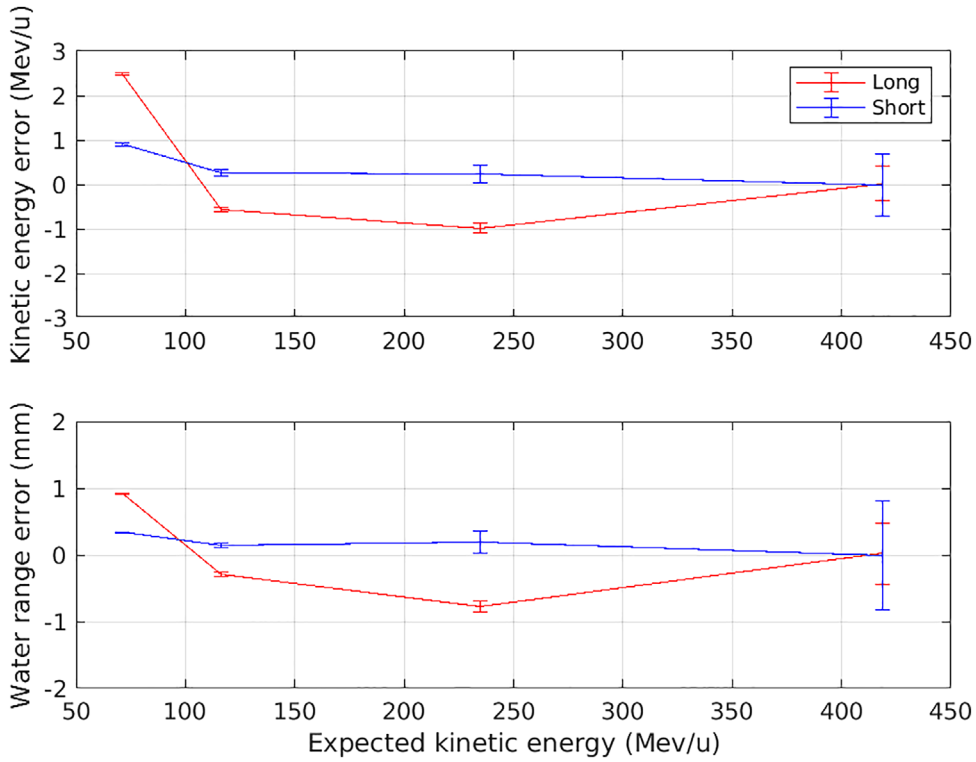

FIGURE 5 (Top) Kinetic energy error for long and short detector separations across five beam energies. Error bars indicate the measurement precision. Deviations were below ± 1 MeV/u for all cases except the 102.56 MeV/u–Long configuration, which showed a 2.5 MeV/u overestimation. (Bottom) Water-equivalent range error with error bars corresponding to the measurement precision. All values remained within ± 1.0 mm, meeting clinical beam-range verification criteria.

A related study by Vignati et al. demonstrated a silicon-based TOF system employing UFSDs based on the low-gain avalanche diode (LGAD) structure. Using a proton therapy beam, the LGAD system achieved a TOF resolution of approximately 3 ps and an energy resolution of 0.2–2.3 MeV at a 36.4 cm sensor distance.[19]

Although this configuration provides excellent timing for single-particle counting, silicon sensors are prone to radiation-induced dopant deactivation (the acceptor removal effect) and lattice defects, which lead to gain degradation and worsening time and energy resolution under high-LET irradiation.[25]

In contrast, the PPC operates through ionization and charge multiplication in a gas medium, where interactions occur only with gas molecules, preventing permanent damage and ensuring stable performance even under high-intensity carbon beam exposure. Similar chamber-type detectors operated with ambient air have already been routinely employed in clinical radiotherapy QA, demonstrating the long-term stability and radiation tolerance of this detector concept.[26,27]

The PPC system demonstrated stable signal amplification and timing performance even under high-LET carbon beam conditions. Furthermore, the applied cross-correlation algorithm, which leverages the entire signal waveform rather than only the leading edge, ensures robust timing determination with reduced sensitivity to pulse variations. When combined with tailored filtering and averaging techniques, this approach provides high timing stability and reproducibility.

From a clinical perspective, the most critical parameter in particle therapy is not the incident beam energy but the range—the stopping depth of particles within the patient. While the incident energy determines the range, dosimetric accuracy and treatment planning are more directly affected by uncertainties in range than by absolute energy values.

In current QA procedures, multilayer ionization chambers (MLICs) such as the Giraffe are widely used for range verification. In contrast, the PPC–TOF system estimates range indirectly through energy measurement, which requires an additional conversion step. Unlike MLICs, however, the PPC is a transmission-type detector that allows the therapeutic beam to pass with minimal perturbation, offering potential for online, three-dimensional beam monitoring. Moreover, when beam-energy drifts or anomalies occur within the nozzle or beamline, the TOF-based system can function as an independent and highly sensitive tool for real-time detection of such deviations.

Future developments should include integration with existing range-verification systems (e.g., Zebra, Giraffe)

and the establishment of accurate TOF–range conversion tables tailored to clinical environments. To accommodate broader irradiation fields, scaling up the detector area will be an important next step.

5 | CONCLUSION

In this study, we present a compact radiation-hard TOF-based energy measurement system for clinical carbon-ion beams using PPC detectors. The system demonstrated reliable timing performance under high-LET irradiation conditions and enabled direct estimation of beam energy using cross-correlation of detector signals. Across the clinical energy range, the measured energies deviated by less than ± 2.5 MeV/u from nominal values, corresponding to a range uncertainty below ± 1 mm—well within clinically accepted criteria.

The PPC-based approach promises a suitable solution for long-term QA applications in carbon-ion beam. Precise and independent verification of beam energy at the delivery point provides a powerful step in delivery assurance that is not fully addressed by existing clinical monitoring systems. Future developments will focus on real-time acquisition integration, detector upscaling, and clinical interfacing with range-verification tools. The results of this work lay a foundation for establishing a detector-driven framework for absolute energy monitoring in CIRT.

ACKNOWLEDGMENTS

This work was supported by Korea Institute for Advancement of Technology (KIAT) grant funded by the government of the Republic of Korea (MOTIE, P0026103), by National Research Foundation of Korea (NRF) Grant funded by the Korean Government (RS-2024-00410034) and by Korea Foundation Of Nuclear Safety (Grant 2205013).

CONFLICT OF INTEREST STATEMENT

The authors declare no conflicts of interest.

REFERENCES

1. Malouff TD, Serago C, Trifiletti DM. A brief history of particle radiotherapy. In: *Principles and Practice of Particle Therapy*. John Wiley & Sons; 2022:1-9. doi:10.1002/9781119707530
2. Amaldi U, Kraft G. Radiotherapy with beams of carbon ions. *Rep Prog Phys*. 2005;68(8):1861-1882. doi:10.1088/0034-4885/68/8/R04
3. Hirao Y, Muramatsu M, Noda K, et al. Heavy ion synchrotron for medical use HIMAC project at NIRS-Japan. *Nucl Phys A*. 1992;538:541-550. doi:10.1016/0375-9474(92)90803-R
4. Particle Therapy Co-Operative Group. Accessed October 11, 2025, https://www.ptcog.site
5. Tsujii H, Kamada T. A review of updated clinical results of carbon ion radiotherapy. *Jpn J Clin Onco*. 2012;42:670-685. doi:10.1093/jjco/hys104
6. Chung SY, Takiyama H, Kang JH, et al. Comparison of clinical outcomes between carbon ion radiotherapy and X-ray radiotherapy for reirradiation in locoregional recurrence of rectal cancer. *Sci Rep*. 2022;12:1845. doi:10.1038/s41598-022-05809-4
7. Patel SH, Wang Z, Wong WW, et al. Charged particle therapy versus photon therapy for paranasal sinus and nasal cavity malignant diseases: a systematic review and meta-analysis. *Lancet Oncol*. 2014;15(9):1027-1038. doi:10.1016/S1470-2045(14)70268-2
8. Rutenberg MS, Beltran C. Future perspective: carbon ion radiotherapy for head and neck and skull base malignancies. *Oral Maxillofac Surg Clin North Am*. 2023;35(3):485-492. doi:10.1016/j.coms.2023.02.009
9. Han MC, Kum WS, Hong C, et al. The first Korean carbon-ion radiation therapy facility: current status of the heavy-ion therapy center at the yonsei cancer center. *Radiat Oncol J*. 2024;42(4):295-307. doi:10.3857/roj.2024.00206
10. Souda H, Yoshida K, Kawashima M, et al. Commissioning and first operation of east japan heavy ion center at Yamagata University. *J Phys: Conference Series*. 2024;2743:012001.
11. Mizushima K, Furukawa T, Noda K, et al. Performance of the HIMAC beam control system using multiple-energy synchrotron operation. *Nucl Instrum Methods Phys Res B*. 2017;406:347-351. doi:10.1016/j.nimb.2017.03.051
12. Sato S, Furukawa T, Noda K. Dynamic intensity control system with RF-knockout slow-extraction in the HIMAC synchrotron. *Nucl Instrum Methods Phys Res A*. 2007;574(2):226-231. doi:10.1016/j.nima.2007.01.174
13. Hiramoto K, Umezawa M, Saito K, et al. The synchrotron and its related technology for ion beam therapy. *Nucl Instrum Methods Phys Res B*. 2007;261(1-2):786-790. doi:10.1016/j.nimb.2007.04.287
14. Magalhaes Martins P, Freitas H, Tessonnier T, Ackermann B, Brons S, Seco J. Towards real-time PGS range monitoring in proton therapy of prostate cancer. *Sci Rep*. 2021;11(1):15331. doi:10.1038/s41598-021-93612-y
15. Idrissi, A.B., Borghi, G., Caracciolo, A. et al. First experimental verification of prompt gamma imaging with carbon ion irradiation. *Sci Rep*. 2024;14(1):25750. doi:10.1038/s41598-024-72870-6
16. Kraan AC, Susini F, Moglioni M, et al. In-beam PET treatment monitoring of carbon therapy patients: results of a clinical trial at CNAO. *Phys Med*. 2024;125:104493. doi:10.1016/j.ejmp.2024.104493
17. Akindinov A, Alici A, Alosi E, et al. The MRPC-based ALICE time-of-flight detector: commissioning and first performance. *Nucl Instrum Methods Phys Res A*. 2012;661:S98-S101. doi:10.1016/j.nima.2010.09.037
18. Colonna N, Barbagallo M, Perea A, et al. Neutron measurements for advanced nuclear systems: the n_TOF project at CERN. *Nucl Instrum Methods Phys Res B*. 2011;269(24):3251-3257. doi:10.1016/j.nimb.2011.04.014
19. Vignati A, Giordanengo S, Milian FM, et al. A new detector for the beam energy measurement in proton therapy: a feasibility study. *Phys Med Biol*. 2020;65:215030. doi:10.1088/1361-6560/abab58
20. Vignati A, Milian FM, Shakarami Z, et al. Calibration method and performance of a time-of-flight detector to measure absolute beam energy in proton therapy. *Med Phys*. 2023;50:5817-5827. doi:10.1002/mp.16637
21. Kwon NH, Choi SW, Han SR, et al. Parallel-plate chambers as radiation-hard detectors for time-based beam diagnostics in carbon-ion radiotherapy. *Nucl Instrum Methods Phys Res A*. 2025;1083:171069. doi:10.1016/j.nima.2025.171069
22. Sun S, Li S, Lin L, et al. A novel signal processing method based on cross-correlation and interpolation for ToF measurement. *Proceedings of the IEEE International Conference on Signal and Image Processing*. 2019:664-668.

23. Queiros R, Alegria FC, Girao PS, Serra ACC. Cross-correlation and sine-fitting techniques for high-resolution ultrasonic ranging. *IEEE Trans Instrum Meas*. 2010;59:3227-3236. doi:10.1109/TIM.2010.2047305
24. IBA Dosimetry. Giraffe multilayer ionization chamber. Schwarzenbruck, Germany. Available at: https://www.iba-dosimetry.com/product/giraffe [accessed 16 Sep 2025]
25. Feng Y, Huang X, Yu C, et al. Study of the acceptor removal effect of LGAD. *IEEE Trans Nucl Sci*. 2022;69:2324-2329. doi:10.1109/TNS.2022.3221482
26. Urakabe E, Inoue M, Iwashita Y, et al. Performance of parallel plate ionization chamber for medical irradiation. In: *Proceedings of the Particle Accelerator Conference. IEEE*. 1997:3819-3821. doi:10.1109/PAC.1997.753426
27. Hamatani N, Yagi M, Shimizu S, Ishino N, et al. Investigation of ionization chamber characteristics for ultrahigh-dose-rate scanned carbon-ion beams. *In Vivo*. 2024;38:2220-2227. doi:10.21873/invivo.13686

How to cite this article: Kwon NH, Choi SW, Han S, et al. Real-time energy measurement of clinical carbon ion beams using a cross-correlation time-of-flight method with parallel-plate chambers. *Med Phys*. 2026;53:e70391. https://doi.org/10.1002/mp.70391